A piezoelectric deformable mirror for intra-cavity laser adaptive optics

Craig S. Long*[a], Philip W. Loveday[a] and Andrew Forbes[b,c]
[a]Sensor Science & Technology, CSIR Material Science and Manufacturing, Box 395, Pretoria 0001, South Africa;
[b]Mathematical Optics, CSIR National Laser Centre, Box 395, Pretoria 0001, South Africa,
[c]School of Physics, University of KwaZulu-Natal, Private Bag X54001, Durban 4000, South Africa

ABSTRACT

This paper describes the development of a deformable mirror to be used in conjunction with diffractive optical elements inside a laser cavity. A prototype piezoelectric unimorph adaptive mirror was developed to correct for time dependent phase aberrations to the laser beam, such as those caused by thermal expansion of materials. The unimorph consists of a piezoelectric disc bonded to the back surface of a copper reflective mirror. The rear electrode of the piezoelectric ceramic disc is divided into segments so that a number of different control voltages can be applied to deform the mirror in a desired displacement distribution. The mirror is required to be able to deform in the shape of each of the lower order Zernike polynomials, which describe aberrations in optical systems. A numerical model of the device was used to determine a suitable electrode configuration. Finally, the device was constructed and the deformed shapes measured using a laser vibrometer.

Keywords: Deformable mirror, adaptive optics, laser beam control, piezoelectric unimorph

1. INTRODUCTION

This paper describes the development of a deformable mirror to be used in conjunction with diffractive optical elements inside a laser cavity. The adaptive mirror will be used to correct for time dependent phase aberrations to the laser beam, such as those caused by thermal effects in the gain material, viz thermal expansion and thermally induced refractive index changes.

For some time, adaptive optics have been used to improve the capabilities of large telescopes by compensating for the effects of air turbulence. Deformable mirrors, actuated by numerous piezoelectric stack actuators have been developed for these telescopes [1]. However, this approach is too bulky and expensive for application inside a laser cavity. Alternatively, compact MEMS mirror arrays are capable of high spatial resolution. Unfortunately, they do not provide sufficient deformation for this application [2]. Piezoelectric unimorph mirrors offer simplicity, compactness, low cost and good displacement amplitude, and were therefore selected for development.

The unimorph consists of a piezoelectric disc bonded to the back surface of the mirror, which could be aluminium, glass or copper. The rear electrode of the piezoelectric ceramic disc is divided into segments each with a corresponding control voltage, in order to deform the mirror in a desired displacement distribution.

In adaptive optics, the imperfections in the optical system, and therefore the deformations that the mirror is required to perform, are often described by Zernike polynomials which are a complete set of orthogonal functions defined on a unit circle. The challenge is to design a device that can represent selected polynomials as accurately as possible, with specified amplitude, while minimizing displacement components attributable to the remaining polynomials.

A numerical model of the device is used to select an appropriate electrode configuration, in order to achieve accurate representation of certain desired shapes. A finite element modelling approach, based on specially formulated hybrid axisymmetric piezoelectric elements with drilling degrees of freedom [3], is employed. A least-squares fit of the deformation of the mirror surface is carried out in order to determine which of the Zernike polynomials are being excited.

* Craig Long <clong@csir.co.za>; phone +27 12 841 2498; fax +27 12 841 3895; www.csir.co.za

Industrial and Commercial Applications of Smart Structures Technologies 2008,
edited by L. Porter Davis, Benjamin Kyle Henderson, M. Brett McMickell, Proc. of SPIE Vol. 6930,
69300Y, (2008) · 0277-786X/08/$18 · doi: 10.1117/12.776178

Finally, a first prototype of the device was constructed and tested. Displacement distributions were measured with a laser vibrometer during development. This allows the voltage ratios for displacing an individual polynomial to be determined and to be compared to the numerical predictions.

2. INTRACAVITY LASER BEAM SHAPING USING DIFFRACTIVE OPTICAL ELEMENTS AND ADAPTIVE OPTICS

The adaptive mirror developed here is ultimately intended for use in intracavity laser beam shaping applications. In this section, some detail regarding the application of diffractive optical elements to intracavity laser beam shaping, and the envisaged role that adaptive optics will play, are presented.

A traditional laser resonator configuration employing a diffractive optical element is depicted in Fig. 1. It consists of a gain medium inside an optical cavity which is supplied with energy. Usually the cavity consists of two mirrors aligned such that the light passes through the gain medium several times, while travelling between the two mirrors. One of the two mirrors is made partially transparent, and the laser beam is emitted through this mirror (henceforth referred to as the output coupler).

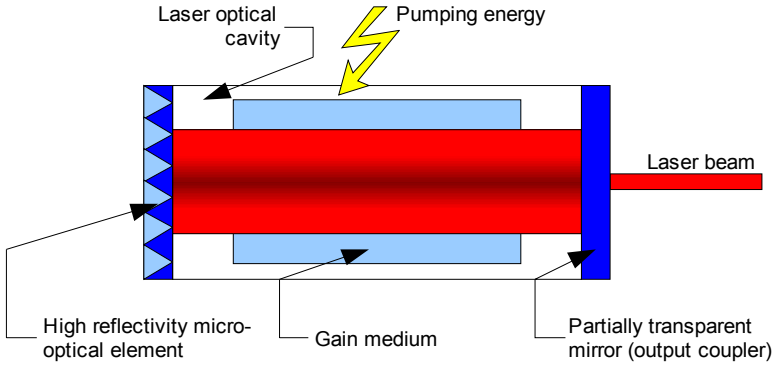

Fig. 1. Laser resonator with a gain medium and a diffractive micro-optical element on the left.

In the case depicted in Fig. 1 the back reflector is a diffractive optical element (DOE); suitable choice of the phase only profile of this element will ensure a customised laser mode at the output coupler [4,5]. This is contrary to conventional resonators with spherical curvature mirrors where only combinations of so–called Helmhotz–Guass beams will resonate (Hermite–Gauss or Legeurre–Gauss modes). Since the laser beam intensity and phase is selected inside the laser by the DOE, this is often referred to as intracavity laser beam shaping. Diffractive optical elements manipulate light by diffraction rather than reflection or refraction, and thus have feature sizes of the order of the wavelength of the light. If the surface structure of the element is of a kinoform nature (continuous relief surface), then the DOE acts as a phase–only element, without any diffraction losses.

In particular, if we describe the desired output field at the output coupler as u_{OC}, then reverse propagating the field to the DOE yields [6]:

$$u_{DOE}(\rho, L) = -i^{n+1}(k/L)\exp(ikL)\exp\left(\frac{ik}{2L}\rho^2\right)\int_0^\infty u_{OC}(r)J_n\left(\frac{k\rho r}{L}\right)\exp\left(\frac{ik}{2L}r^2\right)\exp\left(-\frac{ik}{2f}r^2\right)rdr \qquad (1)$$

where we have assumed that the resonator is rotationally symmetric. Here $k = 2\pi/\lambda$, where λ is the wavelength of the laser beam; ρ, and r are radial co-ordinate variables, and where L is the total optical path length of the resonator. If after refection off the DOE the field u_{DOE} is to reproduce u_{OC} at the output coupler, then the required optical transfer function for DOE mirror must be given by:

$$t_{DOE} = \frac{u^*_{DOE}}{u_{DOE}} \qquad (2)$$

By deforming the DOE, the optical transfer function in (2) can be controlled, thereby modifying the phase of the DOE and consequently the output field u_{OC}. An example of an axisymmetric diffractive optical element is shown in Fig. 2(a), with associated output intensity given in Fig. 2(b). The element was designed for a L = 1.772 m length CO_2 laser cavity, operating at a wavelength of λ = 10.6 μm. The DOE is designed so that a circular super–Gaussian beam is generated at the output coupler, with field given by:

$$u_{OC} = u_0 \exp\left(-(r/w)^{10}\right) \tag{3}$$

with w = 10 mm and u_0 arbitrarily set to 1. Note that the surface height is modulated every 10.6 μm in height, or one complete wavelength, corresponding to a 2π phase shift of the light. This results in the discontinuities in Fig 2(a). Practically it is not necessary to perform the 2π modulation if a continuous surface is easier to fabricate. Because of the small feature sizes of such elements, they are also referred to as micro–optical elements.

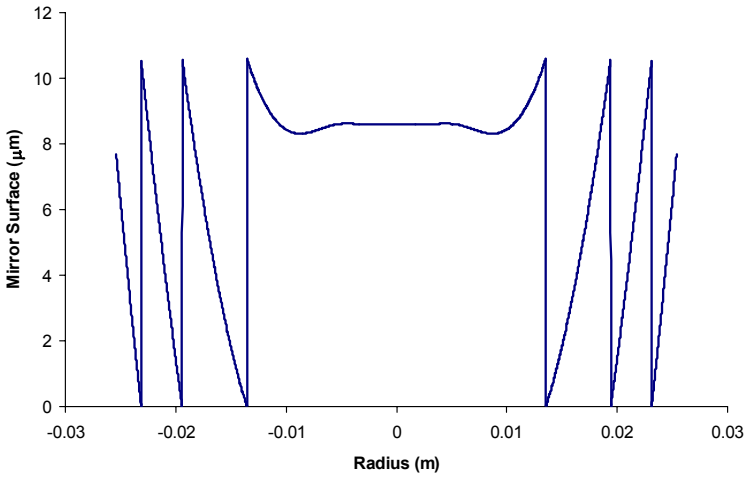

(a) DOE surface, with modulation corresponding to one optical cycle.

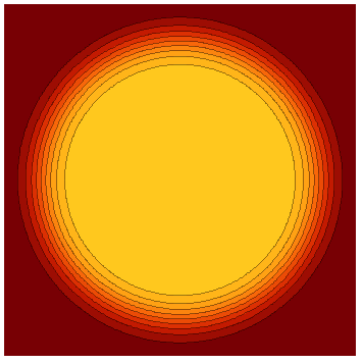

(b) Designed output beam intensity profile, showing a uniform intensity central region and steep edges.

Fig. 2. Example of a DOE for outputting a flat–top beam.

These static micro-optical elements can be designed based on the assumption that the laser resonator parameters do not vary with time. However, non-linear effects within lasers can introduce time dependent phase aberrations to the laser beam, such as thermal expansion of materials, thermal lensing, etc. which depend on the operating parameters of the laser [7].

While certain imperfections can be compensated for during the assembly of the laser, the time dependent imperfections require an adaptive method of compensation [8-12]. Dynamic micro-optical elements, or adaptive mirrors as they are called, can be used to introduce the required phase correction in the system. Furthermore, during the manufacture of these optical elements, some fabrication error is expected, if not likely. An additional application of adaptive optical elements is therefore to compensate for fabrication errors in the imperfect static micro-optical elements. An adaptive mirror would be used to compensate for non-ideal phase due to fabrication errors.

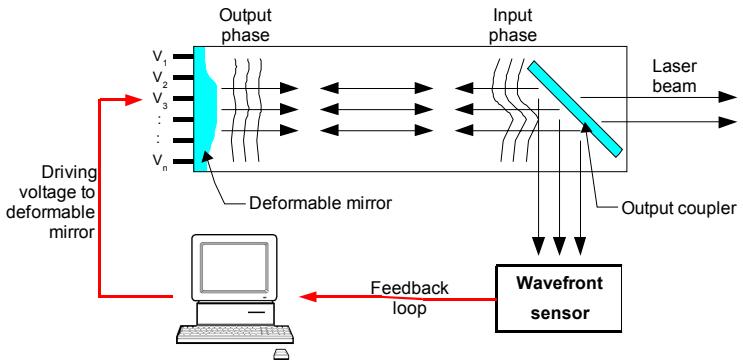

Fig. 3. Schematic of envisaged adaptive optical system.

A schematic illustration of the envisaged arrangement, including the intra-cavity adaptive optical element (deformable mirror), is depicted in Fig. 3. Some light at the output coupler, initially with distorted wavefront, is diverted to a wavefront sensor which extracts the Zernike polynomials describing it. This information is compared to the ideal wavefront, and a prediction of the necessary corrections at the deformable mirror is made. The deformations required by the deformable mirror may then be translated to a voltage applied to each electrode segment on the piezoelectric disc which actuates the mirror. Finally, the adapted shape of the deformable mirror corrects for the initial aberration, improving the output laser beam.

3. PROTOTYPE DEFORMABLE MIRROR

In order to quantify the deformations that are practically feasible from such a deformable mirror, a prototype was designed and manufactured. In this section some details of the construction of the first prototype are provided. This section also discusses the numerical modelling of the device and presents some detail of how the physical device and numerical models are compared using Zernike polynomials.

3.1 Description of unimorph deformable mirror

The prototype unimorph-type deformable mirror consists of a 40 mm diameter, 0.3 mm thick, piezoelectric ceramic disc bonded to a copper disc 44 mm in diameter and 0.3 mm thick. The copper disc was lapped, starting from a 1.2 mm thick flat disc, to ensure flatness and parallelism (see Fig. 4(a)). The slightly larger diameter of the copper provides a surface onto which a grounding wire is attached, as shown in Fig. 4(b).

(a) Deformable mirror prototype (front view).

(b) Deformable mirror prototype (rear view).

Fig. 4. Prototype deformable mirror and experimental setup.

The free electrode on the piezoelectric disc is divided into three concentric rings. The electrode boundaries were positioned where they would be expected to best excite the third Zernike polynomial. Their points were found by solving

$$\frac{d^2 Z_3}{dr^2} = 0 \,, \tag{4}$$

where Z_3 is the third Zernike polynomial. These positions were found to be 0.27×40 mm and 0.72×40 mm respectively. For more details on this procedure, the reader is referred to [13]. The electrode patterning was carried out by laser ablation using an excimer laser. The two discs were then bonded together in a jig to ensure alignment using a thin layer of Hi-Tec polymers AW 106 epoxy. Wires were then soldered to the electrodes.

3.2 Numerical model of deformable mirror

For the purposes of comparison to experimental results an axisymmetric finite element model, using specially developed finite elements with rotational degrees of freedom, was employed. These elements have been shown to be especially well suited to bending-dominated problems such as the one considered here.

The motivation for employing axisymmetric elements with rotational degrees of freedom is similar to the incentive for their use in planar (membrane) elements. Hoop fibre rotational degrees of freedom, schematically illustrated in Fig. 5, are desirable in solid-of-revolution axisymmetric elements to accommodate their connection to axisymmetric shell elements. Furthermore, the accuracy benefits attributed to the enhanced displacement interpolations have been shown to be similar to the planar case.

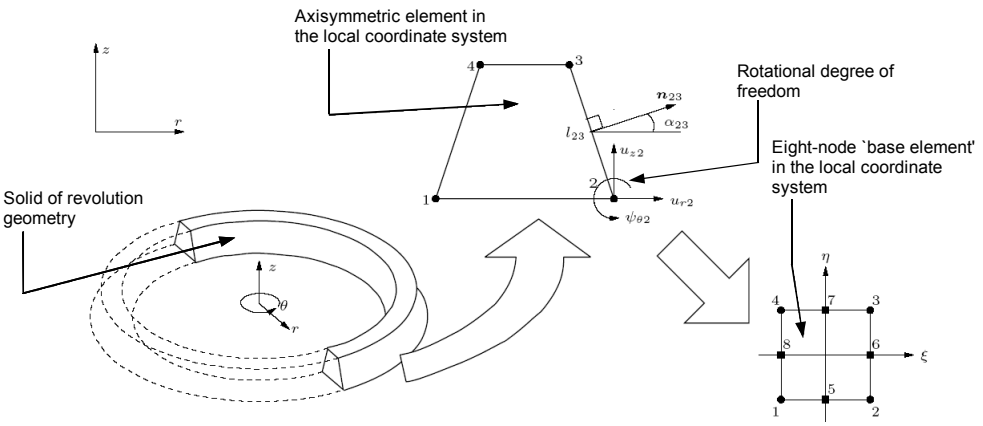

Fig. 5. Quadrilateral axisymmetric element with rotational degrees of freedom.

The variational formulation of these elements employs the skew-symmetric part of the stress tensor as a Lagrange multiplier to enforce the continuum mechanics definition of rotations in terms of displacement gradient. The stress tensor is therefore not a priori assumed to be symmetric. The finite element implementation starts with an eight-node 'base element' in the local coordinate system. The four side nodes are then condensed out, and their normal displacements related to nodal rotations at the four corner nodes, as depicted in Fig. 5.

More detail regarding elastostatic elements of this type may be found in [3]. In order to model the piezoelectrically driven deformable mirror, the elastostatic elements were extended to account for the piezoelectric effect. For brevity, the formulation of the piezoelectric elements with rotational degrees of freedom is not given here. In order to verify the correctness of the finite element implementation described above, results using our code were compared to results using the Comsol Multiphysics commercial software [14], with a very fine mesh and higher-order elements. Good agreement was achieved.

A finite element analysis of the structure photographed in Fig. 4 was carried out. Fig. 6 depicts an example result using the finite element method briefly described above. From this analysis, the vertical displacements of the mirror surface can be extracted. For comparison, and to evaluate the feasibility of the concept, a procedure is now required to determine which of the Zernike polynomials are excited.

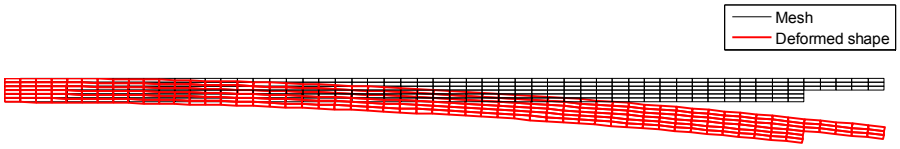

Fig. 6. Typical result using the finite element method, depicting the discretisation and exaggerated deformed shape.

3.3 Zernike polynomial extraction procedure

As mentioned previously, in adaptive optics the spatial deformations that the mirror is required to perform are described using Zernike polynomials, which are a complete set of orthogonal functions defined on a unit circle. The form of the polynomials used in this work is given by:

$$Z_n^m(\rho,\varphi) = R_n^m \cos(m\varphi), \tag{5}$$

with $0 \le \rho \le 1$, $0 \le \varphi \le 2\pi$, and where

$$R_n^m = \sum_{k=0}^{(n-m)/2} (-1)^k \rho^{n-2k} \frac{(n-k)!}{k!\left(\left(n+m/2-k\right)!\left(n-m/2-k\right)!\right)!}. \tag{6}$$

Note that R_n^m is only defined for (n-m) positive and even. Furthermore, due to the symmetry of the problem, only axisymmetric polynomials are considered (i.e. m=0). For brevity, we will denote this subset of Zernike polynomials as

$$Z_i \equiv Z_{n=2i}^{m=0}, \; i=0,1,2,\ldots . \tag{7}$$

In order to determine which of the Zernike polynomials are excited, a least-squares fit of the surface displacements is employed, i.e. we minimize the function

$$\chi^2 = \sum_{i=1}^{N}\left[y_i - \sum\nolimits_{k=0}^{M} a_k Z_k(r_i) \right]^2 , \tag{8}$$

where y_i is the i^{th} of the N surface nodal displacements. The minimization is carried out using the procedure described in [15]. The procedure defines a matrix $\boldsymbol{A}$, the components of which are defined by

$$A_{ij} = Z_j(r_i) . \tag{9}$$

The problem in (8) can now be written in matrix form as

$$\chi^2 = |\boldsymbol{A}\,\boldsymbol{a} - \boldsymbol{y}|^2. \tag{10}$$

Since the pseudoinverse of $\boldsymbol{A}$, denoted $\boldsymbol{A}^{\dagger}$, minimises χ the least-squares fit of the parameters $\boldsymbol{a}$ is given by

$$\boldsymbol{a} = \boldsymbol{A}^{\dagger}\,\boldsymbol{y} . \tag{11}$$

The output of this process is a vector of the coefficients a_k which scale the magnitude of the $M+1$ Zernike polynomial (of which there are only M non-constant polynomials since Z_0=1).

Fig. 7 illustrates a typical result of the polynomial fitting procedure using various numbers of (non-constant) Zernike polynomials, i.e. M = 3, 5, 10 and 20. The figure demonstrates that the error in the fit decreases as the number of polynomials increases, indicating that the procedure has been properly implemented.

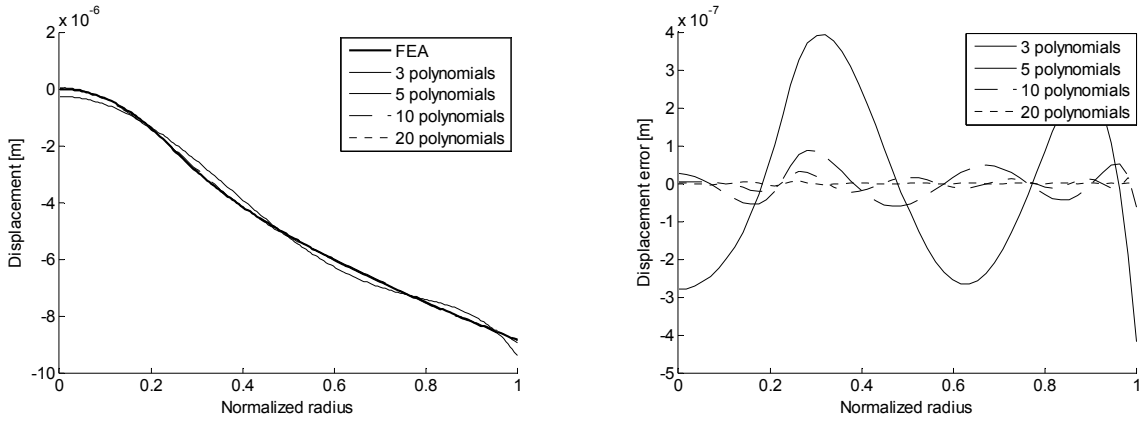

(a) Zernike polynomial fit of finite element results. (b) Error of Zernike polynomial fit.

Fig. 7. Example of Zernike polynomial fitting of finite element prediction of mirror surface using voltage $\boldsymbol{V}_{\text{drive}}$=[100:0:0], see (12).

4. EXPERIMENTAL RESULTS

In this section, the experimental setup used to evaluate the first prototype is described. The experimental results are then compared to numerical results from the model described in Section 3.2.

4.1 Experimental setup

The unimorph is driven by applying prescribed voltages to the segmented electrodes. The voltage used to drive the individual segments is contained in the vector

$$\boldsymbol{V}_{\text{drive}} = [V_1\ V_2\ V_3], \tag{12}$$

where V_1 is the voltage on the inner electrode and V_3 represents the voltage on the outer electrode (see Fig. 4(b)). The voltage is generated using a signal generator at low frequency (200 Hz) and amplified using an AA Lab Systems Ltd. A-303 high voltage amplifier before being applied to the electrodes.

The experimental setup used to measure the surface normal displacement is depicted in Fig. 8(a). Point deformations on the disc are measured using a laser vibrometer. The laser vibrometer consists of a Polytec OFV-505 single point sensor head and the OFV-5000 controller equipped with the VD-06 digital velocity decoder and the DD-500 displacement decoder. A reflective tape was attached to the unimorph, as depicted in Fig. 8(b), to maximise the reflected light detected by the sensor head.

In order to simulate a free boundary condition, the unimorph was simply allowed to rest on a soft cushion. The cushion was contained in a positioning station which manually controlled the position of the polar coordinates of the measurement point.

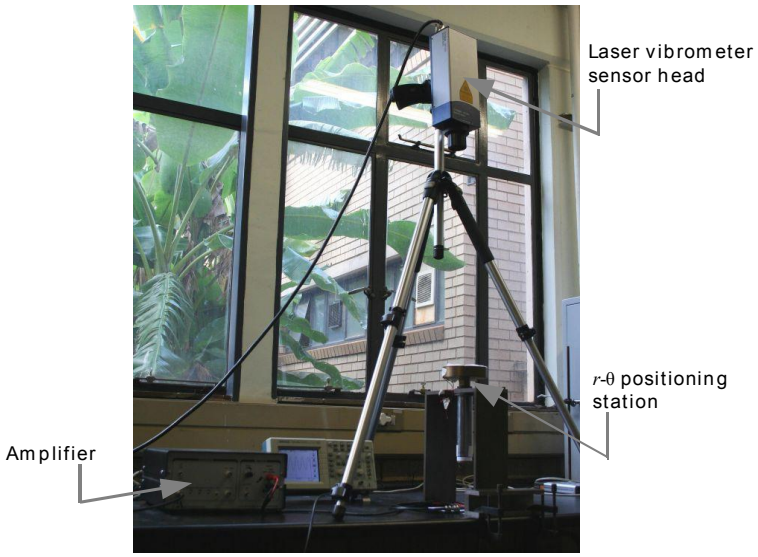

(a) Experimental setup.

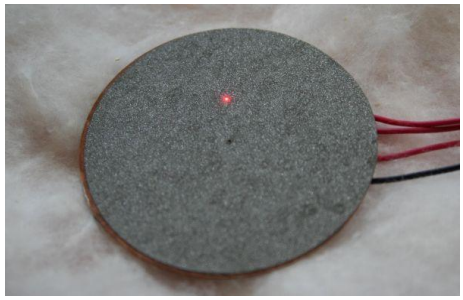

(b) View of unimorph with reflective tape attached.

Fig. 8. Detail of experimental setup.

4.2 Laser vibrometer results

Surface displacement measurements were recorded with each of the three electrodes individually supplied with a 100 V driving voltage, and the remaining two electrodes grounded. The normal displacements were measured on the mirror surface at 12 equally spaced radial positions and at 30º angular increments. The results of these measurements are graphically depicted in Fig. 9, with displacements magnified 1000 times.

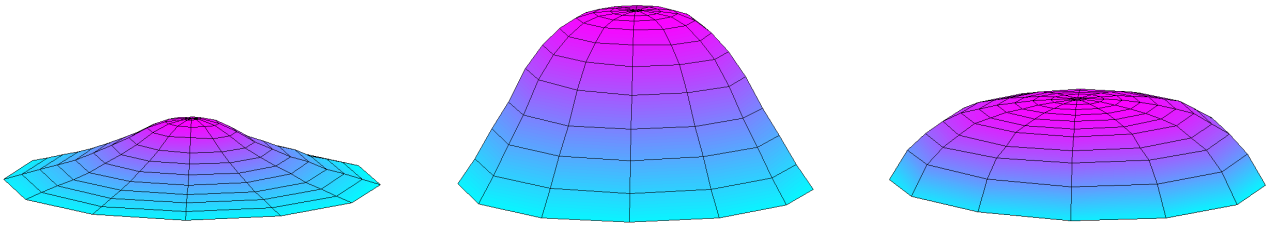

(a) $\boldsymbol{V}_{\text{drive}}$ = [100 0 0]. (b) $\boldsymbol{V}_{\text{drive}}$ = [0 100 0]. (c) $\boldsymbol{V}_{\text{drive}}$ = [0 0 100].

Fig. 9. Measured displacements for driving voltage $\boldsymbol{V}_{\text{drive}}$ amplified 1000 times.

Fig. 10 depicts these same displacements, averaged around the circumference of each measurement radius. The error bars in the figure indicate the magnitude of the departure from this average. As expected, the error increases as the radial distance from the mirror centre increases. The maximum percentage departures from the average displacement recorded were 3.2%, 2.4% and 6.0% for $\boldsymbol{V}_{\text{drive}}$ = [100 0 0], [0 100 0] and [0 0 100], respectively.

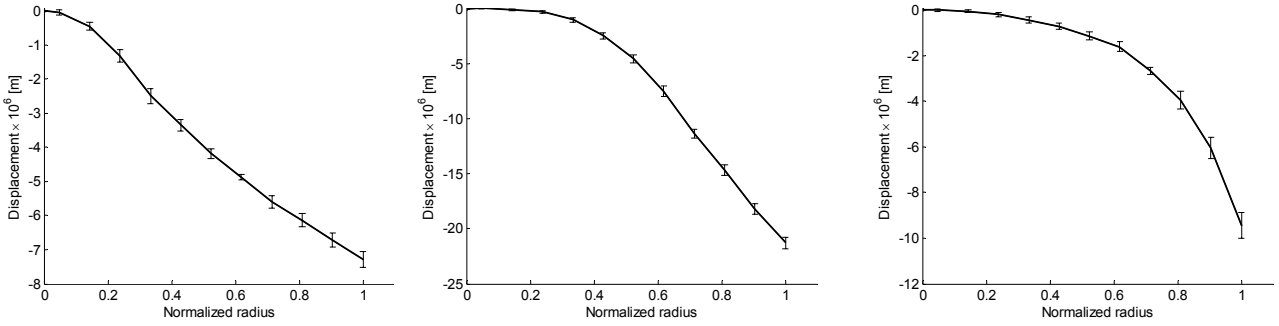

(a) $\boldsymbol{V}_{\text{drive}}$ = [100 0 0]. (b) $\boldsymbol{V}_{\text{drive}}$ = [0 100 0]. (c) $\boldsymbol{V}_{\text{drive}}$ = [0 0 100].

Fig. 10. Variation in displacement, measured at fixed radius, for driving voltage $\boldsymbol{V}_{\text{drive}}$.

4.3 Comparison between experimental and numerical results

Next, the experimental results are compared to the numerical model of the device. Fig. 11 graphically depicts the predicted displacements using finite element analysis, as well as the (average) measured displacements across the mirror surface. Also plotted is the continuous fit of the measured data using the procedure described in Section 3.3.

Qualitatively, the shape of the displacement profile predicted using the finite element method is very similar the measured displacements. However, the magnitude of the predicted displacements are slightly larger. This discrepancy is presumably due inaccuracy in the material properties used for the piezoelectric material in the finite element analysis. The discs were assumed to have properties similar to PZT-5H, but the exact material parameters of the ceramics are not known at this stage.

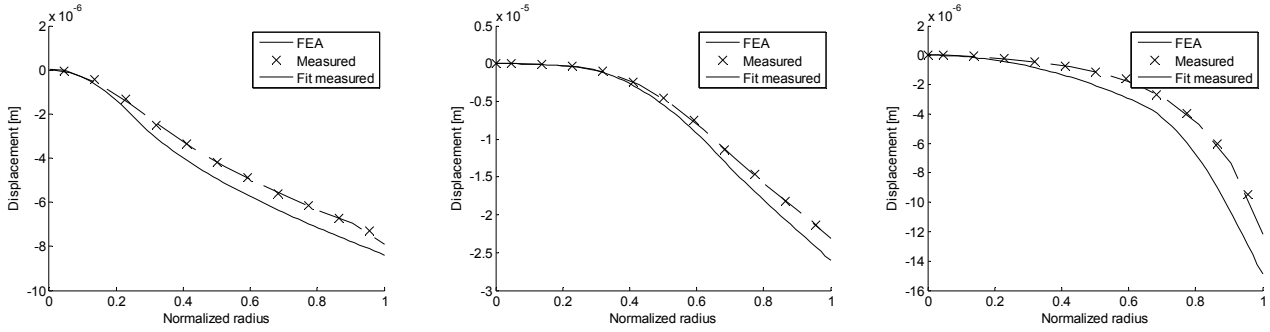

(a) $\boldsymbol{V}_{\text{drive}}$ = [100 0 0]. (b) $\boldsymbol{V}_{\text{drive}}$ = [0 100 0]. (c) $\boldsymbol{V}_{\text{drive}}$ = [0 0 100].

Fig. 11. Comparison between measured and predicted results for driving voltage $\boldsymbol{V}_{\text{drive}}$.

Next, the numerical models are qualitatively compared to experimental data using the coefficients of the Zernike polynomials extracted using the procedure described in Section 3.3. Since the electrode was divided into only three rings, only the first three non-constant Zernike polynomials are reported in the comparison, even though 6 polynomials were extracted.

Table 1 presents the coefficients of the first three non-constant Zernike polynomials, extracted from the experimental results and the finite element model, respectively. Also presented is the percentage difference between the two sets of results, calculated as $((a_{EXP} - a_{FEA}) \div a_{FEA}) \times 100$.

A reasonable correlation between the experimental and numerical results is achieved. As noted previously however, the difference is, in all probability, due to inaccurate piezoelectric material properties used in the finite element analysis. In future, it would be possible to either measure these properties, or simply update the numerical model to account for this error. Since percentage difference between modelled and experimental results are reported in Table 1, the error on polynomials with small coefficients is amplified, even though the absolute error on these terms is acceptable.

Table 1. Coefficients of Zernike polynomials extracted from experimental data and finite element analysis.

Voltage ($\boldsymbol{V}_{drive}$)	Polynomial coefficient	Experimental [µm]	FEA [µm]	Percentage difference [%]
[100 0 0]	a_1	-3.08	-3.22	-4.35
	a_2	1.10	1.32	-16.67
	a_3	-0.68	-0.75	-9.33
[0 100 0]	a_1	-12.67	-14.31	-11.46
	a_2	0.73	0.97	-24.72
	a_3	1.10	1.17	-5.98
[0 0 100]	a_1	-5.45	-7.30	-25.34
	a_2	-2.04	-2.15	-5.12
	a_3	-0.55	-0.28	96.43

4.4 Reduced order model using experimental data

In the adaptive optical system depicted in Fig. 3, it may be beneficial to have a model relating input voltages applied to the piezoelectric electrodes ($\boldsymbol{V}_{drive}$) and the resulting coefficients of the Zernike polynomials describing the mirror surface ($\boldsymbol{a}$). A finite element analysis of the device is one such model, but is far too computationally expensive for closed-loop control. A simple reduced order model would be more appropriate for this application.

To this end, the polynomials extracted from the experimental results may be used to predict the displacements due to an arbitrary driving voltage. Assuming a linear system, a design matrix $\boldsymbol{D}$ can be constructed. The i^{th} column of $\boldsymbol{D}$ consists of the coefficient extracted when a unit driving voltage is applied to electrode i, with the remaining electrodes grounded.

The coefficients predicted using this simple model are then be given by

$$a_i = D_{ij} V_j \,, \quad \text{for } i=1,2,\ldots,M \text{ and } j=1,2,\ldots,N \,, \tag{13}$$

when M Zernike polynomials are extracted and where N represents the number electrodes that can be independently driven. a_i is the predicted amplitude of Zernike polynomial i, when voltage $\boldsymbol{V}_{drive}=[V_1\ V_2\ \ldots\ V_N]$ is applied to the individual electrodes. D_{ij} is the "design matrix" of size $M \times N$.

Table 2 presents the coefficients predicted using (13), and compares them to the measured values, for a driving voltage $\boldsymbol{V}_{drive}=[100\ 100\ 100]$ applied to the electrodes. The percentage error, calculated as $((a_{Predict} - a_{Measured}) \div a_{Measured}) \times 100$ is also presented.

This very simple model (making use of only 3 non-constant Zernike polynomials) achieves good accuracy on the dominant coefficient (a_1) and reasonable accuracy on the others (considering their small amplitudes). One reason for the difference between the results may be attributed to possible non-linear behaviour at high driving voltages.

Table 2. Measured and predicted Zernike polynomial coefficients for $\boldsymbol{V}_{\text{drive}}$=[100 100 100] . Predicted values computed using (13).

Voltage ($\boldsymbol{V}_{\text{drive}}$)	Polynomial coefficient	Predicted [µm]	Measured [µm]	Percentage error [%]
[100 100 100]	a_1	-21.20	-19.54	8.50
	a_2	-0.21	-0.08	162.5
	a_3	-0.13	0.30	-143.3

Note that this method may also be useful for predicting the driving voltage required to achieve a prescribed displacement described using coefficients of the Zernike polynomials. This may be accomplished using

$$V_j = D_{ij}^{-1}\, a_i \,. \tag{14}$$

If D_{ij} is not a square matrix, the pseudo-inverse could be employed to determine the best least-squares fit which would perform the required deformation.

5. CONCLUSION AND RECOMMENDATIONS FOR FUTURE WORK

In this paper the development of a deformable mirror, ultimately intended for use in conjunction with diffractive optical elements inside a laser cavity, is presented. The prototype, piezoelectrically driven, adaptive mirror is being developed to correct for time dependent phase aberrations to the laser beam, such as those caused by thermal expansion of materials.

The unimorph consists of a piezoelectric disc bonded to the back surface of a copper mirror. The rear electrode of the piezoelectric ceramic disc is divided into segments so that a number of different control voltages can be applied to deform the mirror in a desired displacement distribution. The mirror is required to be able to deform in the shape of each of the lower order Zernike polynomials, which describe aberrations in optical systems.

A numerical model of the device using the finite element method was used to determine a suitable electrode configuration. A first prototype of the device was constructed and tested using a laser vibrometer. Good agreement between experimental and numerical results was achieved. In future, the difference between the results could be reduced by employing more accurate material properties in the numerical model. A simple reduced order model for use in a closed-loop control system was also presented and evaluated.

It was shown that a device consisting of two 0.3 mm thick layers can produce the required displacements for correcting aberrations in a CO_2 laser.

Although initial results have been encouraging, significant effort is still required before the development can be considered a success. The next step in the development of the integrated adaptive optical system would therefore involve refining the current prototype.

Specific practical issues which have been encountered during the construction of the first prototype, and which need to be addressed include:

- *Achieving a flat and parallel mirror after polishing.* To achieve large displacements thin discs are required. However, processing (lapping, bonding, soldering, polishing, etc.) these delicate components without resulting in permanent deformation is challenging.
- *Alignment of the two discs during bonding.* Since any misalignment of the two discs would result in non-axisymmetric displacement, careful attention to their alignment is required.

- *Wire attachment.* The soldered joints of the prototype are large when compared to the unimorph thickness, and therefore tend to add significant stiffness locally, again resulting in non-axisymmetric displacements.

Furthermore, significant work is required to incorporate the mirror into a fully functional laser system. Practical issues requiring careful consideration before this step include:

- *Mirror support.* To date laboratory experiments have only been carried out on a freely (or practically freely) supported device. A method for robustly supporting the mirror within the laser cavity is currently being developed.
- *Alignment of the mirror within the laser.* Finally, the alignment of the deformable mirror within the laser cavity is of critical importance if the system is to be practical.

REFERENCES

[1] Tyson, R. Adaptive optics system performance approximations for atmospheric turbulence correction, *Optical Engineering*, **29**, pp. 1165-1173, 1990.

[2] Horsley D.A., Park H., Laut S.P. and Werner J.S., Characterization for vision science applications of a bimorph deformable mirror using phase-shifting interferometry, *Proc. SPIE* **5688**, pp. 133-144, 2005.

[3] Long, C.S., Loveday, P.W. and Groenwold, A.A., Axisymmetric solid-of-revolution finite elements with rotational degrees of freedom, *Finite Elements in Analysis and Design*, Under review (manuscript number L1870).

[4] Belanger P.A., and Pare C., Optical resonators using graded-phase mirrors, *Optics Letters*, **16** (14), 1991.

[5] Pare C. and Belanger P.A., Custom laser resonators using graded-phase mirrors, *IEEE Journal of Quantum Electronics*, **28** (1), 1992.

[6] A.G. Fox, T. Li, Bell Syst. Tech. J. 40 (1961) 453–488.

[7] Forbes A., Botha L.R. Physical optics modelling of intra-cavity thermal distortions in solid state laser resonators, *SPIE* **4768**, pp. 153–163, 2002.

[8] Lee B. et al, Optimization of beam shaping with a dynamic phase spatial light modulator, *Proc. SPIE* **5876**, pp. 603.1 – 603.14, 2005.

[9] Kostylev A. et al, Genetic algorithm for intracavity laser beam shaping, *Proc. SPIE* **5876**, pp. 605.1 – 605.9, 2005.

[10] Sobolev A., et al, Optimised bimorph mirrors for laser beam correction and shaping, *Proc. SPIE* **5876**, pp. 60F.1 – 60F.9, 2005.

[11] Skeren M., et al, Iterative Fourier transform algorithm: different approaches to diffractive optical element design, *Proc. SPIE* **4770**, pp. 75–88, 2002

[12] Cherezova T.Y., et al, Intracavity laser beam shaping by means of a flexible corrector, *Proc. SPIE* **4770**, pp. 96–103, 2002.

[13] Loveday P.W., Long C.S., Forbes, A. and Land, K., Modelling and optimization of a deformable mirror for laser beam control, *Proc. Sixth South African Conference on Computational and Applied Mechanics*, Accepted, to appear, 2008.

[14] http://www.comsol.com/

[15] Ellis, E.M., *Low-cost bimorph mirrors in adaptive optics*, Ph.D thesis, Imperial College of Science, Technology and Medicine, University of London, 1999.

ACKNOWLEDGEMENTS

The authors would like to thank Kevin Land of CSIR, Manufacturing Science and Technology for his assistance in the electrode patterning using excimer laser ablation and for providing access to the Comsol Multiphysics software.